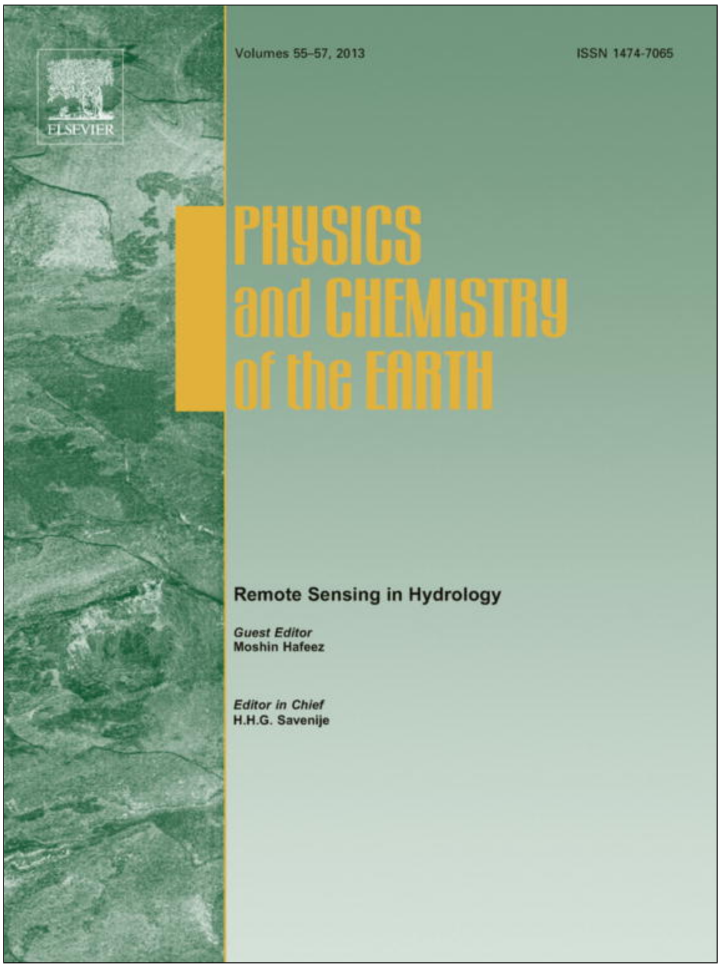
Volumes 55-57, 2013
ISSN 1474-7065
ELSEVIER
PHYSICS
and CHEMISTRY
of the EARTH
Remote Sensing in Hydrology
Guest Editor
Moshin Hafeez
Editor in Chief
H.H.G. Savenije

Physics and Chemistry of the Earth 55-57 (2013) 27–34

Contents lists available at ScienceDirect

Physics and Chemistry of the Earth

journal homepage: www.elsevier.com/locate/pce

Evapotranspiration in the Pampean Region using field measurements and satellite data

Raúl E. Rivas [a,*], Facundo Carmona [a,b]

[a] Comisión de Investigaciones Científicas de Buenos Aires CIC, Instituto de Hidrología de Llanuras IHLLA/Pinto 399, 7000 Tandil, Provincia de Buenos Aires, Argentina
[b] Agencia Nacional de Promoción Científica y Tecnológica de Argentina – ANPCyT/Pinto 399, 7000 Tandil, Provincia de Buenos Aires, Argentina

ARTICLE INFO

Article history:
Received 18 January 2010
Received in revised form 14 September 2010
Accepted 7 December 2010
Available online 13 December 2010

Keywords:
Latent heat flux
Net Radiation
Seguin and Itier equation
Pampean Region

ABSTRACT

Evapotranspiration (*LE*) is an important factor for monitoring crops, water requirements, and water consumption at local and regional scale. In this paper, we applied the semi-empirical model to estimate the daily latent heat flux ($LE_d = Rn_d + A - B(Ts - Ta)$). LE_d has been estimated using satellite images (Thematic Mapper sensor) and a local dataset (incoming and outgoing short- and long-wave radiation) measured during three years. We first estimated the daily net Radiation (Rn_d) from a linear equation derived from the instantaneous net Radiation ($Rn_d = CRn_i + D$). Subsequently, coefficients *A* and *B* have been estimated for two different cover vegetations (pasture and soybean). For each vegetation cover, an error analysis combining Rn_d, *A*, *B*, and surface and air temperatures has been calculated. Results showed that Rn_d had good performance (nonbias and low RMSE). LE_d errors for pasture and soybean were ±28 W m^{-2} and ±40 W m^{-2} respectively.

1. Introduction

Evapotranspiration (*ET*) is a primary process driving energy and water exchange among the hydrosphere, the atmosphere, and the biosphere (Priestley and Taylor, 1972; Brutsaert, 1984). *ET* is an important factor for monitoring water requirements of crops and water consumption at local and regional scale. Different methods have been proposed for measuring *ET* on various spatial scales from individual plants (i.e. porometer, sap-flow, lysimeter), fields (i.e. field water balance, Bowen ratio, scintillometer, eddy correlation) or landscape scales (i.e. energy balance, catchment water balance) (Soegaard and Boegh, 1995; Wang et al., 2006). Satellite Remote Sensing (*RS*) is a promising tool which has been used to provide reasonable estimates of the actual *ET* (also denoted as *LE*) at regional scales. Most *LE* estimations from *RS* can be calculated as a residual term of the available surface energy (*Rn*), the sensible heat flux (*H*), and the ground heat flux (*G*):

$$Rn = LE + G + H \quad (1)$$

Rn and *H* are calculated by a set of variables, some of which can be instantaneously estimated by *RS* (albedo, emissivity, and radiometric surface temperature). For most *RS*-based energy balance studies, it is assumed that *Rn* and *G* are known or they might be easily computed. The two remaining terms, *H* and *LE*, whose estimations are very difficult, are turbulent flux quantities. These terms are usually modeled using one-dimensional flux-gradient expressions based on a convection analogue to Ohm's law:

$$H = \frac{\rho C_p}{r_a}(T_0 - T_a) \quad (2)$$

$$LE = \frac{\rho C_p}{\gamma}\frac{(e_0 - e_a)}{(r_v + r_a)} \quad (3)$$

where ρ is the air density, C_p is the specific heat of the air, T_0 and e_0 are, respectively, the aerodynamic temperature and the vapor pressure of the surface at the effective level of heat and moisture exchange, T_a and e_a are the temperature and the vapor pressure of the overlying atmosphere, r_a and r_v are, respectively, the aerodynamic and physiological resistances to heat and moisture transport at the surface, and γ is the psychrometric constant.

Eqs. (1) and (2) form the basis of the alleged one-layer (*OL*) energy balance models. There is no distinction made in those models among vegetation canopy energy balance, temperature and vapor pressure regimes, and soil surface. To overcome the problem related to the lack of information on the surface resistance, *LE* (Eq. (3)) is estimated as the residual term (Eq. (1)). *RS* has been widely used with this type of framework to estimate the turbulent flux component of the surface energy balance. To do this, radiometric surface temperature (*Ts*) obtained from *RS* is used as a substitute for T_0 in Eq. (2) (Jackson et al., 1977; Seguin and Itier, 1983; Inoue and Moran, 1997; Sanchez et al., 2008a,b). The r_a is usually estimated using meteorological local data on wind speed, stability

* Corresponding author.
E-mail addresses: rrivas@rec.unicen.edu.ar (R.E. Rivas), facundo.carmona@rec.unicen.edu.ar (F. Carmona).

1474-7065/$ - see front matter © 2010 Elsevier Ltd. All rights reserved.
doi:10.1016/j.pce.2010.12.002

conditions, and roughness length, even though the average area of roughness lengths is highly nonlinear.

Over the last years, several regional experiments have tested *OL* models in detail and have provided significant progress (Gourturbe et al., 1997; Kustas and Norman, 1999). At the same time, results from these experiments have allowed to find feebleness in *OL* models and have pointed keys for future research. In fact, two alternative models including representations of different temperature and energy balance regimes for the vegetation canopy and the soil surface have been developed (Choudhury and Monteith, 1988; Kustas, 1990; Zhao-Liang et al., 2009). These models are considerably more complex, although recent investigations have shown them to be successful in overcoming some of the limitations of *OL* models. These models require in situ measurements (net Radiation, air temperature, air relative humidity, wind speed, crop height and leaf area index, canopy and soil temperatures, height and architecture of the plants, among others) and this information is not available in many situations. However, in many standard meteorological stations, there is not instrumentation to measure all these variables required by the models. The lack of specific instrumentation considerably limits the use of sophisticated models and operational applications. Moreover, these models are often limited due to the inherent complexity of those procedures. In most cases, however, regional values are estimated by semi-empirical models using as input local flux data measurement and *RS*. (Zhao-Liang et al., 2009; Reginato et al., 1985; Caselles and Delegido, 1987; Vidal and Perrier, 1989; Kustas et al., 1994). Jackson et al. (1977) were the first to demonstrate from field experiment that *LE* rates directly correlate with the temperature difference between canopy surface (*Ts*) and air (*Ta*). Seguin and Itier (1983) modified this method with the following semi-empirical model to calculate daily *LE* from:

$$LE_d - Rn_d = A - B(Ts - Ta) \tag{4}$$

where Rn_d is daily net Radiation, A is a simple partition into unstable case ($Ts - Ta > 0 \rightarrow A \neq 0$) and the advective case ($Ts - Ta < 0 \rightarrow A = 0$), and slope B is defined as a mean exchange coefficient which is weighted by the ratio between Rn_d and instantaneous net Radiation (Rn_i). B is indeed related to the instantaneous sensible heat flux (Eq. (2)) and can be defined as $B \cong Rn_d Rn_i^{-1} \rho Cp r_a^{-1}$, where r_a depends on wind velocity and a roughness parameter (Seguin and Itier, 1983).

In Eq. (4), daily G is considered equal to zero (Jackson et al., 1977; Seguin and Itier, 1983), and A and B coefficients are considered to be constants at regional level for practical use (Seguin and Itier, 1983; Vidal and Perrier, 1989).

Semi-empirical models in flat areas are good tools for *LE* estimation (Brasa et al., 1998; Seguin et al., 1982) and good alternatives for regions with a lack of specific instrumentation. These models are also applicable in regions such as the Pampean Region of South America, where there can be seen homogeneous extended covers of soybean, maize, wheat, barley, oat, alfalfa, and others.

The objectives of this study are: (1) to obtain, from radiation measurement at local scale for the Pampean Region of Argentina, a relationship between daily net Radiation (Rn_d) and instantaneous net Radiation (Rn_i), (2) to validate the relationship Rn_d–Rn_i, (3) to estimate A and B coefficients (Eq. (4)) for soybean (*Glycine max* (L.) Merrill) and pasture (*Dactylis glomerata*, *Festuca arundinacea* and *Lolium multiflorum*), and (4) to apply the semi-empirical model with Landsat Thematic Mapper (TM) data.

2. Materials and methods

2.1. Experimental site and used datasets

The experiment was carried out in Argentina at a flat subhumid site (average slope of less than 1%) in the Salado River basin (37°5′ S, 59°7′ W, elevation 130 m) on 121 clear days between 2006 and 2009 in two plots of an homogeneous pasture and soybean stands with a full canopy cover (Fig. 1a). The average annual rainfall is about 950 mm (Tandil Station of the Argentinean National Meteorological Network, 37°14′ S and 59°15′ W, elevation 175 m), where the maximum monthly value is in March and the minimum is in August. Average values for annual temperature, wind speed, relative air humidity, and solar radiation are 14.2 °C, 2.6 m s^{-1}, 83% and 186 W m^{-2}, respectively. The average annual evapotranspiration is 1015 mm.

An energy balance station was located within a plot area of 5 ha of pasture and a 16 ha one of soybean. Short-wave (up and down) and long-wave radiation (up and down) were measured with a net radiometer (CNR1 Kipp & Zonnen through short-wave CM3 and long-wave CG3 radiation sensors). Air temperature/relative humidity and wind speed/direction were also measured (CS215-L16 Temperature and RH Probe Campbell Scientific, Met One 034B Windset Campbell Scientific). All data were obtained at 2 m high and recorded at 15 min intervals in a data logger (CR10X Campbell Scientific) (Fig. 1b).

Two TM images from the same area were acquired during the period of highest development of soybean and medium development of pasture. These had a 30 m resolution (band 6 is resampled to 30 m), seven band, 20 km × 20 km subsets of TM scenes acquired by the Landsat 5 satellite on March 3 and 19, 2007 (Fig. 1c). The full scene location reference was path 225 and row 86 on the Landsat World-wide Reference System. The images have been rectified by a reference image after atmospheric correction.

2.2. Estimation of the actual daily evapotranspiration

The actual daily evapotranspiration (LE_d) was calculated from the model proposed by Seguin and Itier (1983):

$$LE_d = Rn_d + A - B(Ts_i - Ta_i) \tag{5}$$

where Rn_d (W m^{-2}) is daily net Radiation, A (W m^{-2}) and B (W m^{-2} °C^{-1}) are empirical coefficients obtained for the study area, and Ts_i and Ta_i are, respectively, the instantaneous surface and the air temperature (°C).

The Rn_d can be obtained from the instantaneous net Radiation (Rn_i) estimated using satellite data. To obtain this information, it is necessary to know the relationship between the instantaneous and daily value of Rn. To estimate Rn_d, we assume that:

$$Rn_d = Rn_{10-11}C + D \tag{6}$$

where Rn_{10-11} is the average Rn registered between 10:00 am and 11:00 am, and C (dimensionless) and D (W m^{-2}) are coefficients obtained from a linear regression between the local measures registered of Rn_d and Rn_{10-11} through a CNR1 sensor in the pasture and soybean plots.

Rn_d and Rn_{10-11} have been determined according to the following expression through CM3 and CG3 sensors:

$$Rn = Rs_{\downarrow} - Rs_{\uparrow} + Rl_{\downarrow} - Rl_{\uparrow} \tag{7}$$

where $Rs_{\downarrow}$ is the incoming short-wave radiation (W m^{-2}), $Rs_{\uparrow}$ is the outgoing short-wave radiation (W m^{-2}), $Rl_{\downarrow}$ is the incoming long-wave radiation (W m^{-2}), and $Rl_{\uparrow}$ is the outgoing long-wave radiation (W m^{-2}).

A and B were statistically determined from a linear regression of LE_d–Rn_d values versus the corresponding Ts_i–Ta_i measurements at a local scale assuming homogeneous surface (Wassenaar et al., 2002). LE_d has been calculated from the Penman Monteith (PM) equation (Allen et al., 1998) using meteorological data recorded by an energy balance station.

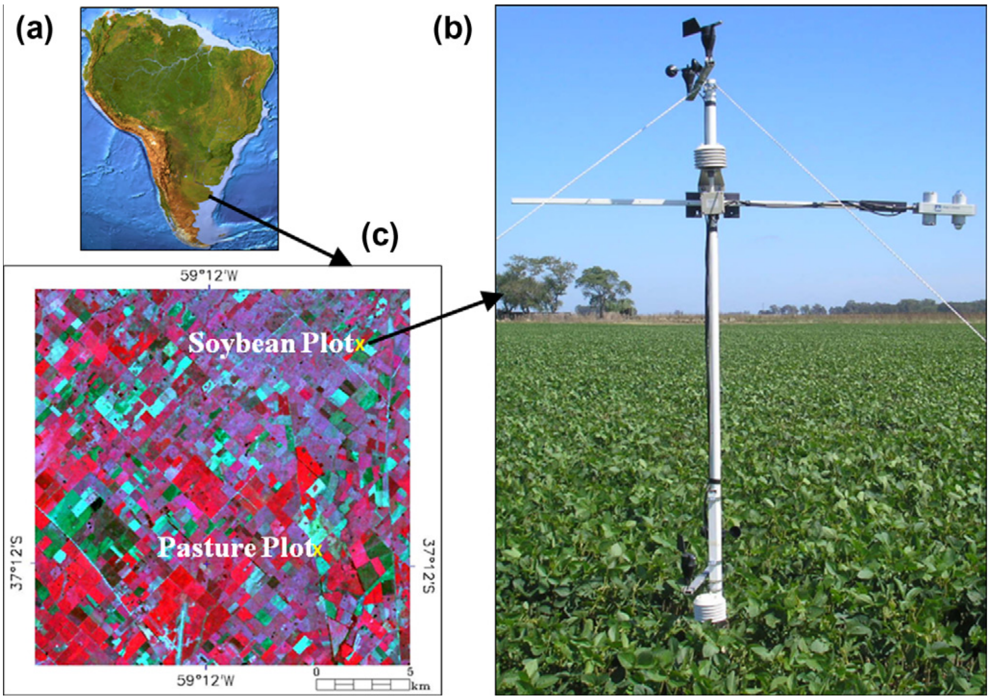

Fig. 1. General location map (a), meteorological station at the soybean plot (b), and composite subset false color image (TM sensor) showing study area (c).

2.3. Estimation of the net instantaneous radiation

The solar instantaneous Radiation (Rs_i) was assumed constant for the study area (Lagouarde and Brunet, 1993; Caselles et al., 1998). For every pixel, the Rn_i has been calculated by satellite data (TM sensor) from:

$$Rn_i = Rs_i(1 - \alpha) + \varepsilon_s \varepsilon_a \sigma T_a^4 - \varepsilon_s \sigma T_s^4 \quad (8)$$

where α is the albedo of the surface (dimensionaless), ε_a is the emissivity of the atmosphere (dimensional), ε_s is the emissivity of the surface (dimensionless), σ is the Stephan–Boltzmann's constant (W m^{-2} K^{-4}), T_a (K) is the air temperature measured at 2 m at the moment of the overpass satellite, and T_s (K) is the surface temperature.

Rs_i was obtained as the average $Rs_\downarrow$ registered between 10:00 am and 11:00 am by the CM3 up sensor.

α was determined from the surface reflectance of the bands 1–5 and 7 ($\rho_{\lambda S}$, being λ band number), in agreement with the method of Starks et al. (1991):

$$\alpha = \pi(0.111\rho_{1S} + 0.119\rho_{2S} + 0.078\rho_{3S} + 0.124\rho_{4S} + 0.041\rho_{5S} + 0.019\rho_{7S}) \quad (9)$$

Eq. (10) was used to obtain the surface reflectance of bands 5 and 7, and Eq. (11) to estimate the surface reflectance of bands 1–4 (assuming a uniform Lambertian surface under cloudless conditions) (Schroeder et al., 2007).

$$\rho_{\lambda AS} = \frac{\pi L_{\lambda sensor}}{E_{\lambda 0} d^{-2} \cos\theta_z} \quad (10)$$

$$\rho_{\lambda S} = \frac{\pi(L_{\lambda sensor} - L_{\lambda p})}{T_{\lambda v}(E_{\lambda 0} d^{-2} \cos\theta_z T_{\lambda z} + E_{\lambda down})} \quad (11)$$

where $\rho_{\lambda AS}$ is the at-satellite reflectance (considered equal to $\rho_{\lambda S}$ for the bands 5 and 7), $L_{\lambda sensor}$ is the at-satellite radiance (W m^{-2} sr^{-1} μm^{-1}), d is the Earth–Sun distance in astronomical units (au), $E_{\lambda 0}$ is the exoatmospheric solar irradiance (W m^{-2} μm^{-1}), θ_z is the zenithal solar angle, $L_{\lambda p}$ is the path radiance (W m^{-2} sr^{-1} μm^{-1}), T_v is the atmospheric transmittance from the target toward the sensor, T_z is the atmospheric transmittance in the direction of illumination and $E_{\lambda down}$ is the downwelling diffuse irradiance (W m^{-2} μm^{-1}).

To derive values of the atmospheric correction coefficients $T_{\lambda z}$, $T_{\lambda v}$, $E_{\lambda down}$, and $L_{\lambda p}$ in Eq. (11), we used the *Dark Object Subtraction* (DOS) method (Schroeder et al., 2007; Song et al., 2001).

The ε_a has been calculated from T_a (Brutsaert, 1984):

$$\varepsilon_a = \frac{0.92}{10^5} T_a^2 \quad (12)$$

Surface emissivity has been determined from satellite images using the Fractional Vegetation Cover (*Fr*) for every pixel as input information. The equation for vegetable covers of extensive crops (wheat, barley, alfalfa, soybean and pasture, among others) is (Valor and Caselles, 1996; Rivas and Caselles, 2004):

$$\varepsilon_s = \varepsilon_v Fr + \varepsilon_{so}(1 - Fr) \quad (13)$$

where ε_v is the emissivity of the vegetation and ε_{so} is the soil emissivity.

The *Fr* has been obtained from the equation of Carlson and Ripley (1997):

$$Fr = \left(\frac{NDVI - NDVI_{\min}}{NDVI_{\max} - NDVI_{\min}}\right)^2 \quad (14)$$

where $NDVI_{\min}$ and $NDVI_{\max}$ correspond to the values of *NDVI* for bare soil (*NDVI* → *minimum*) and a surface with a *Fr* of 100% (*NDVI* → *maximum*).

2.4. Estimation of the surface temperature

The T_s (corrected of the atmospheric effects) has been calculated from the temperature of the satellite (T_{sensor}), applying the single-channel method proposed by Jiménez-Muñoz and Sobrino (2003):

$$T_s = \gamma[\varepsilon^{-1}(\psi_1 L_{sensor} + \psi_2) + \psi_3] + \delta \quad (15)$$

with

$$\gamma = \left\{ \frac{c_2 L_{sensor}}{T_{sensor}^2} \left[\frac{\lambda_{ef}^4}{c_1} L_{sensor} + \lambda_{ef}^{-1} \right] \right\}^{-1} \tag{16a}$$

$$\delta = -\gamma L_{sensor} + T_{sensor} \tag{16b}$$

where L_{sensor} (W m^{-2} sr^{-1} μm^{-1}) is the at-sensor radiance, T_{sensor} (K) is the at-sensor brightness temperature, λ_{ef} is the effective wavelength (11.457 μm for band 6, TM sensor), $c_1 = 1.19104 \times 10^8$ W μm^4 m^{-2} sr^{-1}, and $c_2 = 14387.7$ μm K. The atmospheric functions ψ_1, ψ_2 and ψ_3 have been obtained as a function of the total atmospheric water vapor content (w) (Jiménez-Muñoz and Sobrino, 2003). The w values were considered as the average measurements in the surroundings of the stations of Ezeiza (34°49′ S, 58°32′ W, elevation 20 m) and Santa Rosa (36°34′ S, 64°16′ W, elevation 191 m), Argentina, at 12:00 pm for the considered dates (*University of Wyoming, Department of Atmospheric Science*, http://weather.uwyo.edu/upperair/sounding.html).

3. Results and discussion

3.1. Experimental determination of the coefficients C and D

From the CNR1 sensor, radiation of 121 clear days has been obtained in the period 2006–2009. Fig. 2 shows the annual evolution of Rn_d (cross symbol) and Rn_{10-11} (triangle symbol) for pasture and soybean. Fig. 3 indicates that the ratio Rn_d/Rn_i is not constant throughout the year. Therefore, it is necessary to find a function that relates the daily and instantaneous Rn along the year. Table 1 provides a summary for the statistics illustrated in Figs. 2 and 3.

Fig. 4 shows Rn_d as a function of Rn_{10-11} for 80 clear days of the dataset. Rn_d and Rn_{10-11} are linearly related ($r^2 = 0.971$) for the 80 day period already discussed.

Then, the result of the model proposed (Eq. (6)) for the dataset showed in the Fig. 4 is:

$$Rn_d = Rn_{10-11} 0.43 - 54 \tag{17}$$

where $C = 0.43 \pm 0.01$ (dimensionless) and $D = 54 \pm 3$ (W m^{-2}).

From Eq. (6), a sensitivity analysis of the model was carried out. Subsequently, the error in Rn_d was determined from this equation by applying the error theory as:

$$\delta Rn_d = [(\delta Rn_{10-11} C)^2 + (Rn_{10-11\max} \delta C)^2 + (\delta D)^2]^{1/2} \tag{18}$$

where δRn_d is the error of Rn, $Rn_{10-11\max}$ is the maximum value of Rn registered between 10:00 and 11:00 am, and δC and δD are the errors in C and D, respectively. If we consider that $Rn_{10-11\max} = 589$ W m^{-2}, $\delta Rn_{10-11\max} = 59$ W m^{-2}, $\delta C = 0.01$ and $\delta D = 3$ W m^{-2}, we obtained $\delta Rn_d = 26$ W m^{-2} as the error of the model.

In order to validate the linear Rn_d equation, a comparison was made between Rn_d measured by the CNR1 and Rn_d estimated from our proposed model (Eq. (6)) for a set of 41 data. Fig. 5 evidences the comparative results of the 41 values measured and calculated. Taking into account the 41 datasets, it may be noticed that the proposed model presents a rather low bias (2 W m^{-2}) and RMSE of ± 12 W m^{-2}.

3.2. Estimation of the coefficients A and B for vegetation covers of pasture and soybean

The semi-empirical coefficients A and B were found using values of LE_d from PM, daily values of Rn, and measurement of $Ts_i - Ta_i$ (measures at midday) for every clear day, from 36 data for pasture and 11 data for soybean plots. Figs. 6 and 7 show the results of daily $LE - Rn$ as a function of canopy – air temperature difference.

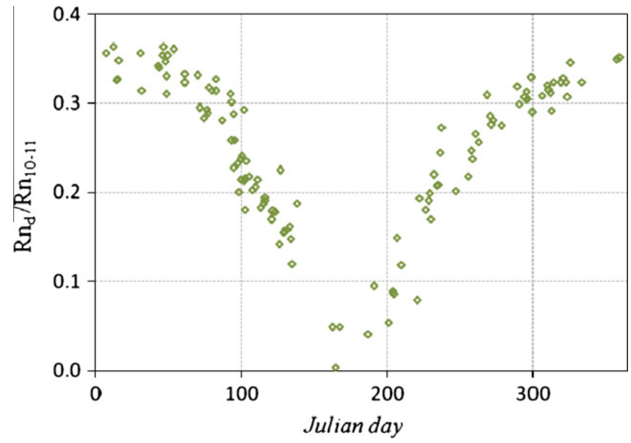

Fig. 3. Relationship Rn_d/Rn_{10-11} as a function of Julian days.

Table 1
Descriptive statistics of Rn_d, Rn_{10-11} and Rn_d/Rn_{10-11} considering clear days only.

Variable	Average	Standard deviation	Minimum	Maximum
Rn_d (W m^{-2})	98	61	−11	201
Rn_{10-11} (W m^{-2})	356	142	121	589
Rnd/Rn_{10-11}	0.24	0.10	−0.08	0.36

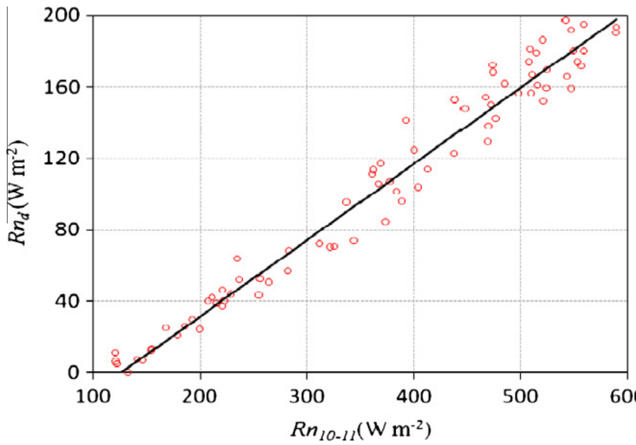

Fig. 4. Rn_d as function of Rn_{10-11} and linear regression.

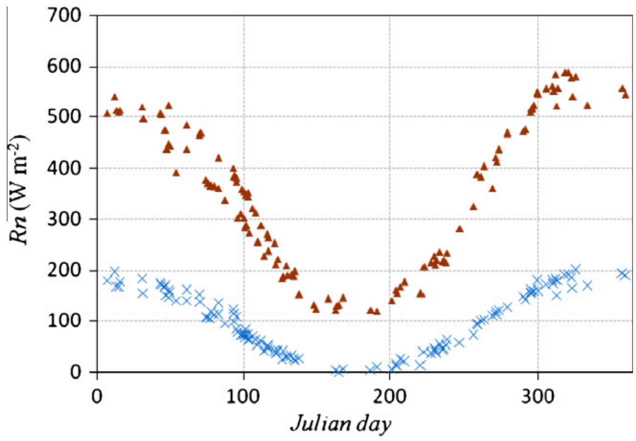

Fig. 2. Rn_d (X) and Rn_{10-11} (▲) as a function of Julian days.

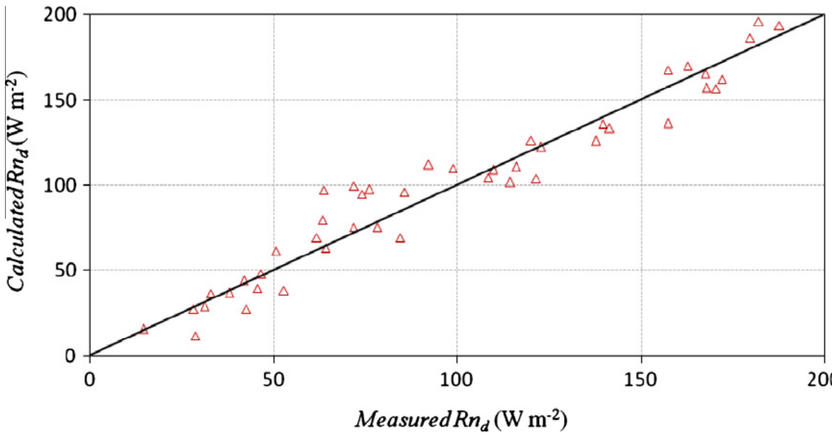

Fig. 5. *Calculated* Rn_d versus *Measured* Rn_d. The 1:1 line is also shown.

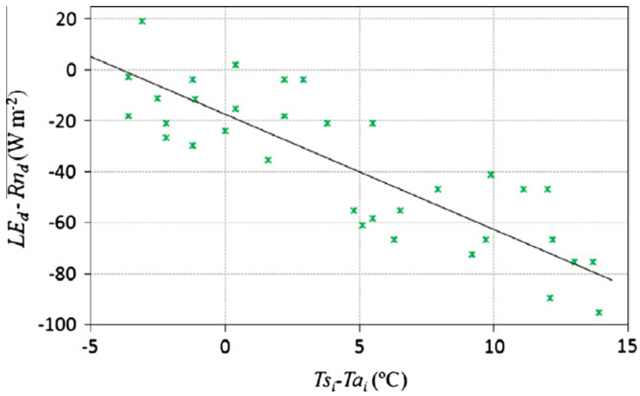

Fig. 6. Relationship between $(LE_d - Rn_d)$ versus $(Ts_i - Ta_i)$ for plots under pasture.

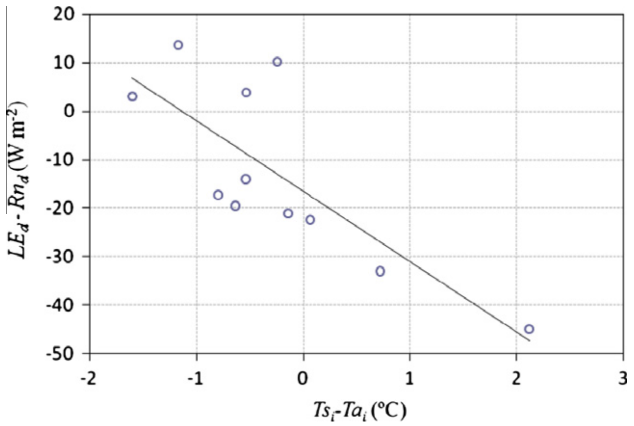

Fig. 7. Relationship between $(LE_d - Rn_d)$ versus $(Ts_i - Ta_i)$ for the plots under soybean.

For the pasture plots dataset (Fig. 6), the A, B, and determination coefficient (r^2) obtained are: $A = -17 \pm 3$ (W m^{-2}), $B = 4.5 \pm 0.4$ (W m^{-2} °C^{-1}) and $r^2 = 0.75$.

For the soybean plots dataset (Fig. 7), the A, B, and determination coefficient (r^2) obtained are: $A = -16.5 \pm 3.8$ (W m^{-2}), $B = 14.6 \pm 3.9$ (W m^{-2} °C^{-1}) and r^2 of 0.61.

A values obtained in the settings reported no stability conditions ($Ts - Ta > 0$) for the two plots in question, while B exchange coefficient is higher in soybean (14.6 W m^{-2} °C^{-1}) and lower in pasture (4.5 W m^{-2} °C^{-1}). These results indicate, for the two cases, typical values of A and B corresponding to unstable conditions (pasture and soybean non-irrigated).

From Eq. (5), a sensitivity analysis of the model was conducted. The error in LE_d pasture and soybean was obtained as:

$$\delta LE_d = [(\delta Rn_d)^2 + (\delta A)^2 + ((Ts_i - Ta_i)_{\max}\delta B)^2 + B(\delta Ts_i)^2 + B(\delta Ta_i)^2]^{1/2} \tag{19}$$

where δA, δB, δTs_i, and δTa_i are, respectively, the errors in A, B, Ts (single-channel method, TM sensor), and Ta (CS215-L16 Temperature and RH Probe Campbell Scientific). $(Ts_i - Ta_i)_{max}$ is the biggest difference between temperatures of surface and air in every cover. If we assumed the values reported in Table 2, the errors of the LE_d model using satellite data are ±28 W m^{-2} and ±40 W m^{-2} for pasture and soybean respectively. If we assumed Rn_d equals 200 W m^{-2} and the LE_d error is the previously indicated, then LE_d estimated map errors are 14% (soybean) and 20% (pasture).

3.2.1. LE_d maps from Landsat TM

In the experimental area, we used a crop map obtained combining the bands $\rho_{\lambda 3}$, $\rho_{\lambda 4}$, $\rho_{\lambda 5}$ and $\rho_{\lambda 7}$. For the classification, we used the image of March 19, to which a mask of cities and small water bodies had previously been applied (using ground truth from an agricultural region of 150 km by 100 km). To the image stemming from this procedure, a supervised classification was applied using

Table 2
Values used in the Eq. (19).

Surface	$A \pm \delta A$ (W m^{-2})	$B \pm \delta B$ (W m^{-2} °C^{-1})	$(Ts_i - Ta_i)_{\max}$ (°C)	δTs_i (°C)	δTa_i (°C)
Pasture	−17.5 ± 3.3	4.5 ± 0.5	14.4	2	0.2
Soybean	−16.5 ± 3.8	14.6 ± 3.9	2.1	2	0.2

Table 3
Accuracy of each class using a Maximum Likelihood classification.

Class	Accuracy (%)	Pixel number				
		Soybean	Pasture I	Pasture II	Corn	Bare soil
Soybean	90	87	0	0	0	0
Pasture I	100	0	184	0	0	0
Pasture II	77	0	0	59	0	18
Corn	100	0	0	0	162	0
Bare soil	100	0	0	0	0	77

Overall accuracy: 95%; kappa coefficient: 0.94

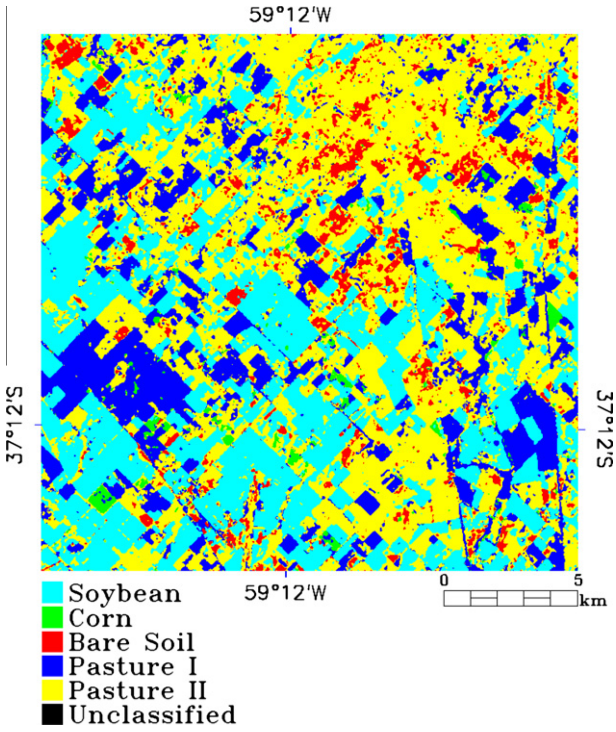

Fig. 8. Results of classifications by means of applying the Maximum Likelihood method on March 19, 2007.

the Maximum Likelihood method, using 5 classes. The defined ground truth classes were: soybean, bare soil, corn, pasture I (pasture in lowlands) and pasture II (pasture in highlands). The overall accuracy of the expert classification was 95% and the individual class accuracy ranged from 77% to 100% for each class (Table 3). Fig. 8 shows the classified image after removing boundary effects using a medium filter (3 × 3).

LE_d maps have been obtained by means of applying Eq. (5), using Rn_d and T_s estimated from TM sensor data (Eqs. (6), (8), and (15)), semi-empirical coefficients (A and B) for pasture and soybean, and local data (Rs_i and T_a) (Table 4).

Figs. 9 and 10 show LE_d spatial variability of pasture and soybean across the tested area during days March 3 and 19, 2007. In Fig. 9, the results of applying a mask to Fig. 8 are shown. In this Figure, LE_d is displayed throughout pastures during these two days. In Fig. 10, the mask has been applied in order to display, in this case, LE_d soybean results for the above mentioned days.

LE_d values along the pasture showed a minimum of 89 W m^{-2}, a maximum of 149 W m^{-2} and a average of 113 ± 13 W m^{-2} on 03 March (Fig. 9a) and a minimum of 83 W m^{-2}, a maximum of 137 W m^{-2} and a average of 106 ± 11 W m^{-2} on 19 March (Fig. 9b).

For soybean the results showed a minimum of 65 W m^{-2}, a maximum of 170 W m^{-2} and a average of 133 ± 24 W m^{-2} on 03 March (Fig. 10a) and a minimum of 52 W m^{-2}, a maximum of 131 W m^{-2} and a average of 102 ± 16 W m^{-2} on 19 March (Fig. 10b).

Finally, we compared LE_d measured at the local plots (applying LE_d–PM with meteorological data and soil moisture) (Soybean and

Table 4
Data used to obtain LE_d maps.

Date	Surface	Rs_i (W m^{-2})	T_a (°C)	ε_v	ε_{so}	ε_a	$NDVI_{min}$	$NDVI_{max}$	W (g cm^{-2})
03 March 2007	Pasture	757	22.0	0.975	0.960	0.801	0.212	0.908	1.576
	Soybean	757	22.0	0.985	0.960	0.801	0.212	0.908	1.576
19 March 2007	Pasture	688	23.6	0.975	0.960	0.810	0.075	0.870	1.913
	Soybean	688	23.6	0.985	0.960	0.810	0.075	0.870	1.913

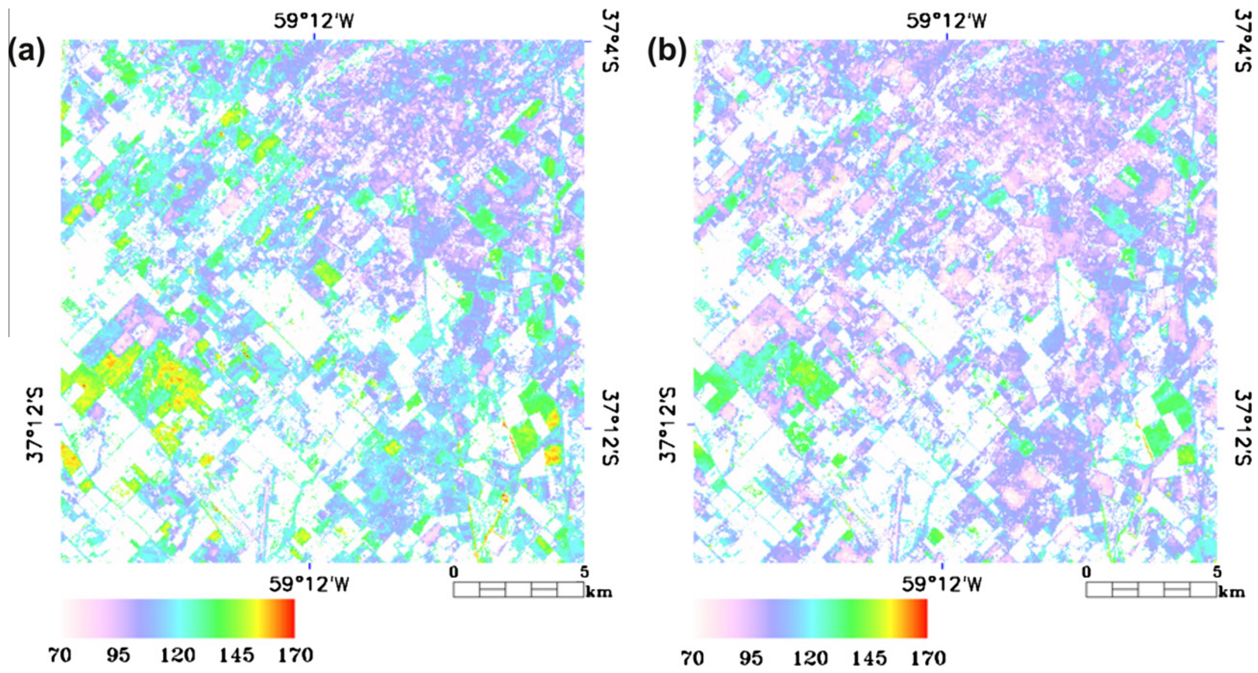

Fig. 9. LE_d pasture: (a) March 03 and (b) March 19, 2007. Values in W m^{-2}.

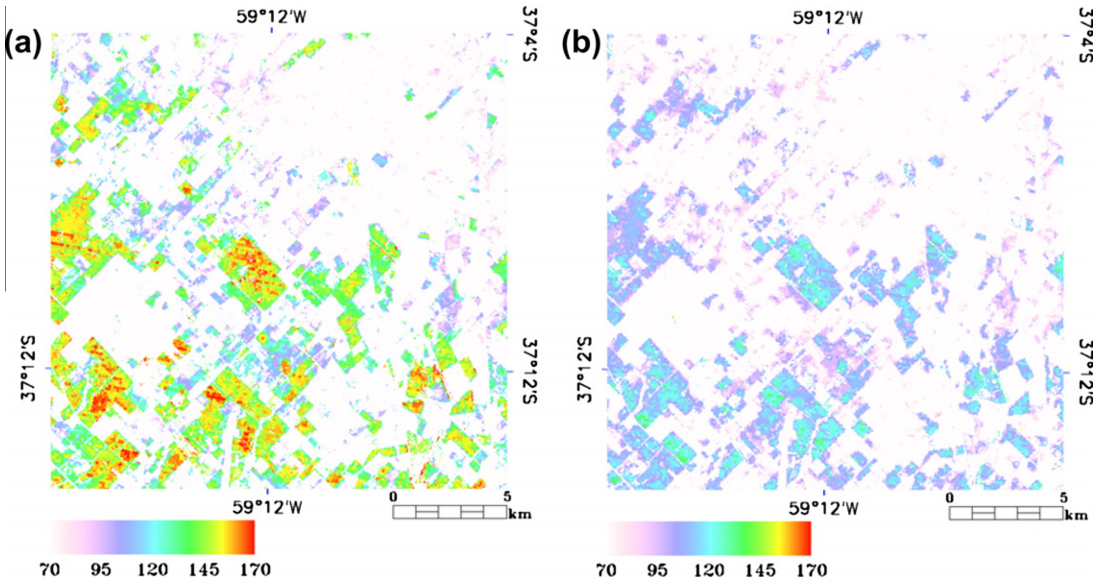

Fig. 10. LE_d soybean: (a) March 03 and (b) March 19. Values in W m^{-2}.

Table 5
Comparison between local LE_d and modeled LE_d (Eq. (5)).

Date	Surface	LE_{dlocal} (W m^{-2})	LE_{dModel} (W m^{-2})
03 March 2007	Pasture	102	116
	Soybean	124	135
19 March 2007	Pasture	113	102
	Soybean	138	126

Pasture) with what was obtained by means of the Eq. (5) (Table 5) from the images. Despite the limited number of data for ground validation, these four data show some interesting features. For example, the latent heat flux is different in the pasture and Soybean at local scale when applying the model but the LE_d values are not different enough to obtain conclusions. It is interesting to point out that the model proposed by Seguin and Itier (1983) has captured the LE_d variation. These results are further improved by conducting more measures through the LE_d Soybean and Pasture in local plots.

4. Conclusions

In this work, the semi-empirical model of Seguin and Itier (1983) has been applied using a linear function ($Rn_d = Rn_{10-11}C + D$) to estimate the Rn_d from the Rn_i obtained by means of satellite. The Rn_d validation with information measured in pasture and soybean in the Pampean Region of Argentina does not exhibit a significant deviation and the RMSE is ±12 W m^{-2}. In addition, the function is valid for low and high values of Rn.

With the measured data in a CNR1 sensor, the coefficients of LE_d model for the analyzed covers have been estimated, giving values of A and B of -17.5 ± 3.3 W m^{-2} and 4.5 ± 0.4 W m^{-2} °C^{-1} for the pasture and -16.5 ± 3.8 W m^{-2} and 14.6 ± 3.9 W m^{-2} °C^{-1} for the soybean, respectively. As the availability of meteorological stations is very dense (taking into account the stations of the National Agricultural Technology Institute, Argentinean National Meteorological Network and universities, among others) the applicability of the model in the region is ensured.

LE_d maps obtained for two different summer dates of 2007, applying TM sensor images, presented errors of 14% for pasture and of 20% for soybean.

The equation developed to estimate Rn_d is valid to be applied in the Pampean Region by means of data acquired from other sensors (e.g. AVHRR and MODIS), which must allow obtaining surface temperature (captured between 10:00 and 11:00 am) and albedo.

Acknowledgements

This work was financed by the Agencia Nacional de Promoción Científica y Tecnológica de Argentina (Project ANCPyT/PICTO 22825), the Comisión de Investigaciones Científicas de Buenos Aires, the Universidad Nacional del Centro de la provincia de Buenos Aires (Project I020) and a Research Grant of Mr. F. Carmona (Agencia Nacional de Promoción Científica y Tecnológica de Argentina-PRH 0032). We wish to thank the Comisión Nacional de Actividades Espaciales de Argentina (CONAE) for providing the satellite TM data.

References

Allen, R.G., Pereira, L.S., Raes, D., Smith, M., 1998. Crop evapotranspiration-Guidelines for computing crop water requirements-FAO. Irrigation and drainage. In: Water Resources, Development and Management Service, Rome, Italy. Paper 56, pp. 323.

Brasa, A., Martín de Santa Olalla, F., Caselles, V., Jochum, M., 1998. Comparison of evapotranspiration estimates by NOAA-AVHRR images and aircraft flux measurement in a semiarid region of Spain. J. Agric. Eng. Res. 70, 285–294.

Brutsaert, W., 1984. Evaporation into the atmosphere. Theory, History, and Applications. Reidel Publishing Company, Dordrecht, Holland. pp. 299.

Carlson, T.N., Ripley, D.A., 1997. On the relation between NDVI, fractional vegetation cover, and leaf area index. Remote Sens. Environ. 62, 241–252.

Caselles, V., Delegido, J., 1987. A simple model to estimate the daily value of the regional maximum evapotranspiration from satellite temperature and albedo images. Int. J. Remote Sens. 8, 1151–1152.

Caselles, V., Artigao, M., Hurtado, E., Coll, C., Brasa, A., 1998. Mapping actual evapotranspiration by combining Landsat TM and NOAA-AVHRR images: Application to the Barrax area, Albacete, Spain. Remote Sens. Environ. 63, 1–10.

Choudhury, B., Monteith, J., 1988. A four-layer model for the heat budget of homogeneous land surfaces. Q. J. Roy. Meteorol. Soc. 114, 373–398.

Gourturbe, J., Lebel, T., Dolman, A., Gash, J., Kabat, P., Kerr, Y., Monteny, B., Prince, S., Stricker, J., Tonga, A., Wallace, J., 1997. An overview of HAPEX-Sahel: a study in climate and desertification. J. Hydrol. 189, 4–17.

Inoue, Y., Moran, M.S., 1997. A simplified method for remote sensing of daily canopy transpiration- A case study with direct measurements of canopy transpiration in soybean canopy. Int. J. Remote Sens. 18 (1), 139–152.

Jackson, R.D., Reginato, R.J., Idso, S.B., 1977. Wheat canopy temperature: a practical tool for evaluating water requirements. Water Resour. Res. 13, 651–656.

Jiménez-Muñoz, J.C., Sobrino, J.A., 2003. A generalized single channel method for retrieving land surface temperature from remote sensing data. J. Geophys. Res., 108.

Kustas, W., 1990. Estimate of evapotranspiration with a one and two layer model of heat transfer over partial canopy cover. J. Appl. Meteorol. 29, 704–715.
Kustas, W.P., Norman, J.M., 1999. Evaluation of soil and vegetation heat flux predictions using a simple two-source model with radiometric temperatures for a partial canopy cover. Agric. For. Meteorol. 94, 13–29.
Kustas, W.P., Blanford, J.H., Stannard, D.I., Daughtry, C.S.T., Nichols, W.D., Weltz, M.A., 1994. Local energy flux estimates for unstable conditions using variance data in semiarid rangelands. Water Resour. Res., 1351–1361.
Lagouarde, J.P., Brunet, Y., 1993. A simple model for estimating the daily upward longwave surface radiation flux from NOAA-AVHRR data. Int. J. Remote Sens. 14 (5), 907–925.
Priestley, C., Taylor, R., 1972. On the assessment of surface heat flux and evaporation using large-scale. Mon. Weather Rev. 100, 81–92.
Reginato, R.J., Jackson, R.D., Pinter, J.P., 1985. Evapotranspiration calculated from remote multispectral and ground station meteorological data. Remote. Sens. Environ. 18, 75–89.
Rivas, R., Caselles, V., 2004. A simplified equation to estimate spatial reference evaporation from remote sensing-based surface temperature and local meteorological data. Remote Sens. Environ. 93, 68–76.
Sanchez, J.M., Scavone, G., Caselles, V., Valor, E., Copertino, V.A., Telesca, V., 2008a. Monitoring daily evapotranspiration at a regional scale from Landsat-TM and ETM + data: Application to the Basilicata region. J. Hydrol. 351, 58–70.
Sánchez, J.M., Kustas, W.P., Caselles, V., Anderson, M.C., 2008b. Modelling surface energy fluxes over maize using a two-source patch model and radiometric soil and canopy temperature observations. Remote Sens. Environ. 112, 1130–1143.
Schroeder, T.A., Cohen, W.B., Song, C., Canty, M.J., Yang, Z., 2007. Radiometric correction of multi-temporal Landsat data for characterization of early successional forest patterns in western Oregon. Remote Sens. Environ. 103, 16–26.
Seguin, B., Itier, B., 1983. Using midday surface temperature to estimate daily evaporation from satellite thermal IR data. Int. J. Remote Sens. 4, 371–383.
Seguin, B., Itier, B., Monget, J.M., Petit, V., 1982. Utilisation de la thermographie IR poer l'estimation régionale. Mise au Point Méthodologique Sur Le Site de la Crau, Agronomie 2 (1), 7–16.
Soegaard, H., Boegh, E., 1995. Estimation of evapotranspiration from a millet crop in the Sahel combining sap flow, leaf area index, and eddy correlation technique. J. Hydrol. 166, 265–282.
Song, C., Woodcock, C.E., Seto, K.C., Pax-Lenney M Macomber, S.A., Macomber, M., 2001. Classification and change detection using Landsat TM data: When and how to correct atmospheric effects? Remote Sens. Environ. 75, 230–244.
Starks, P.J., Norman, J.M., Blad, B.L., Walter-Shea, E.A., Walthall, C.L., 1991. Estimation of shortwave hemispherical reflectance (albedo) from bidirectionally reflected radiance data. Remote Sens. Environ. 38, 123–134.
Valor, E., Caselles, V., 1996. Mapping land surface emissivity from NDVI: Application to European, African and South American areas. Remote Sens. Environ. 57, 167–184.
Vidal, A., Perrier, A., 1989. Analysis of a simplified relation for estimating daily evapotranspiration from satellite thermal IR data. Int. J. Remote Sens. 10, 1327–1337.
Wang, K., Li, Z., Cribb, M., 2006. Estimation of evaporative fraction from a combination of day and night land surface temperatures and NDVI: A new method to determine the Priestley–Taylor parameter. Rem. Sens. Environ. 102, 293–305.
Wassenaar, T., Olioso, A., Hasager, C., Jacob, F.A., 2002. Estimation of evapotranspiration on heterogeneous pixels. In: Recent Advances in Quantitative Remote Sensing. Publications Universitat de València, Spain. p. 458–465.
Zhao-Liang, L., Ronglin, T., Zhengming, W., Yuyun, B., Chenghu, Z., Bohui, T., Guangjian, Y., Xiaoyu, Z., 2009. A review of current methodologies for regional evapotranspiration estimation from remotely sensed data. Sensors 9, 3801–3853.